Combined effects of curvature, radiation, and stretch on the extinction of premixed tubular flames

Zheng Chen *, Yiguang Ju [1]

Department of Mechanical and Aerospace Engineering, Princeton University, Room D115, E-Quad, Olden Street, Princeton, NJ 08544, USA

ABSTRACT

The combined effects of flame curvature, radiation, and stretch on the extinction of premixed tubular flames are investigated by using the large-activation-energy asymptotic method with a non-linear radiation model. A general expression for flame speed, flame temperature and extinction limits is obtained and it is used to study the radiation and flame curvature coupling at different Lewis numbers. The results show that the coupling between radiation and flame curvature leads to multiple flame bifurcations and extinction limits. Furthermore, both the stretch and radiation extinction limits are found to be greatly affected by flame curvature.

© 2008 Elsevier Ltd. All rights reserved.

1. Introduction

The recent industrial interest in ultra lean coal gasified syngas combustion in gas turbines creates a need to understand the near limit flame dynamics to improve the flame stability and to reduce emissions. Unlike the conventional fuels, coal syngas contains a significant amount of radiative gases such as CO, CO_2 and H_2O. In addition, curved flame fronts prevail in turbulent combustion and the effect of curvature on flame propagation is important, especially for near limit flames. Therefore, in order to extend the flammability and to improve the flame stability, it is particularly important to understand how the coupling of thermal radiation, flame curvature, and stretch affects the flame speed and extinction limits.

It is well known that radiation heat transfer is a dominant mechanism for near limit flames. Indeed the flammability limit is determined by the radiation heat loss for unstretched premixed planar flames [1,2]. However, for stretched flames, the flammability limit can be changed through the combined effects of thermal radiation and flame stretch. The combined effects of flame radiation and stretch have been studied by using planar and radiative counterflow flames [3–12]. These studies have shown that the flammability limit of stretched flames below a critical Lewis number can be lower than that of unstretched flames. The extended flammable region is found due to the existence of the Near Stagnation plane Flame (NSF) and the flammability of the stretched flame

below the critical Lewis number is characterized by the limit of the NSF [9]. The flammable region of premixed counterflow flames is bounded by the stretch extinction limit at large stretch rate and the radiation extinction limit at low stretch rate. Numerical simulations [8,9] further demonstrated that multi-flame bifurcations are intrinsic phenomena caused by the combined effects of radiation and flame stretch, and the limits of these flame regimes are sensitive to the Lewis numbers of reactants and to radiation heat losses.

For curved flames, the combined effects of flame stretch and curvature have been studied experimentally, theoretically and numerically by using tubular flames [13–21]. Tubular flames, which can be well established in laboratory, provide a simple configuration to study the fundamental behavior of the flames subject to a curvature. It has been shown that flame curvature and Lewis number strongly affect the extinction of tubular flames and flame extinction is also characterized by the limit of the NSF. Unfortunately, radiation heat loss, which is crucial to the extinction of near limit flames, has not considered in the above tubular flame studies because of the difficulty in experiments. In examining the effect of flame cooling on the extinction of the tubular flame, earlier studies focused on the effect of heat loss to the wall [15,20]. The combined effect of radiation heat loss with stretch and curvature, however, has not been addressed in all the previous studies except for the numerical study by Ju et al. [22].

Ju et al. [22] investigated the interaction between radiation heat loss and flame curvature numerically by using premixed tubular CH_4/air flames. The results show that the interaction of flame curvature and radiation heat loss greatly affects the flame strength and extinction. Unfortunately, the numerical simulations did not

---

* Corresponding author. Tel.: +1 609 258 1411; fax: +1 609 258 6109.
  E-mail addresses: zhengc@princeton.edu (Z. Chen), yju@princeton.edu (Y. Ju).
[1] Tel.: +1 609 258 5644; fax: +1 609 258 6109.

provide an explicit correlation between the extinction limits and the individual parameters corresponding to flame curvature, radiation, and stretch, which is very important for parameter selection in engine design and fire safety control. In Ref. [22], the flame curvature changed together with stretch, therefore the effect of different curvatures at the same stretch rate on flame extinction could not be demonstrated. Furthermore, the numerical simulations were limited to CH_4/air mixtures, and the effect of Lewis number remains unclear. Therefore, to gain a clear understanding of the extinction mechanism and to obtain an explicit correlation of the flammability limit, it is necessary to perform an analytical study to investigate the combined effects of curvature, radiation, stretch, and Lewis number on flame extinction.

The purpose of the present study is to provide a general theoretical description of the combined effects of flame curvature, radiation, and stretch as well as preferential diffusion on the extinction of premixed flames. Radiative premixed tubular flames at different curvatures and planar counterflow flames without curvature are analyzed by using the asymptotic strategy. First, the mathematical model is given. Then, the asymptotic solutions of the radiative tubular and counterflow flames are presented. Finally, the combined effects of curvature, radiation, stretch, and Lewis number on flame extinction are discussed.

2. Mathematical model

In order to study the effect of flame curvature, two kinds of flame configurations are considered in this study. The first one is the premixed tubular flame shown in Fig. 1(a). Combustible mixture is injected toward the concentric inner tube (stagnation surface) from the inner wall of the porous outer tube. A positively stretched tubular flame with well defined flame curvature can be stabilized between the inner and outer tubes [14,17–19]. The inner tube is introduced here to change the flame curvature [17–19,21]. The second configuration is the premixed planar counterflow flame shown in Fig. 1(b). This flame is also positively stretched but has no flame curvature. Therefore, by comparing the flame dynamics of these two flames at the same stretch rate and radiation intensity,
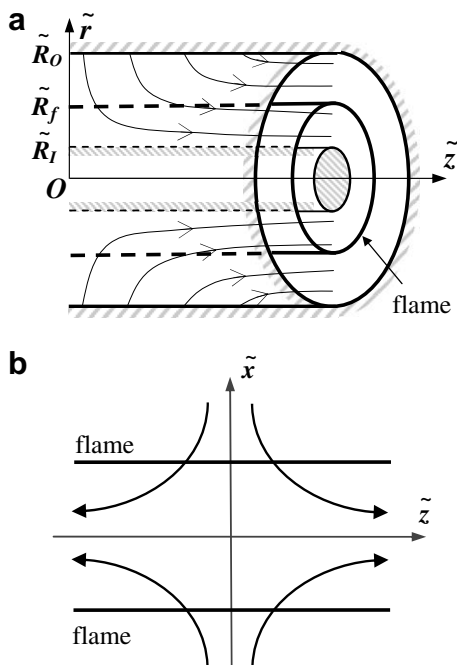

Fig. 1. The schematic diagrams of (a) the tubular flame and (b) the counterflow flame.

the curvature effect on the near limit radiative flames can be readily demonstrated.

For both flame geometries, the potential flow assumption, which is commonly used in the large activation energy asymptotic analysis [3,10,20], is employed here. By introducing a geometry factor N with $N = 0$ for the counterflow flame and $N = 1$ for the tubular flame (with $\widetilde{R}_I$ and $\widetilde{R}_O$ being the inner and outer tube radius, respectively), the potential flow field for both configurations can be written as

$$\tilde{u} = -\tilde{k}(\tilde{r}^2 - \widetilde{R}_I^2)/[(1+N)\tilde{r}] \tag{1a}$$

$$\tilde{w} = \tilde{k}\tilde{z} \tag{1b}$$

where $\tilde{u}$ and $\tilde{w}$ are velocities in the radial ($\tilde{r}$-axis for tubular flame with $N = 1$, $\tilde{x}$-axis for counterflow flame with $N = 0$, $\tilde{x} = \tilde{r}$, $\widetilde{R}_I = 0$, and $\widetilde{R}_O \to \infty$) and the axial directions ($\tilde{z}$-axis), respectively, and $\tilde{k}$ is the inlet velocity gradient.

According to the definition of flame stretch rate [23] and the simplified expression derived by Matalon [24], flame stretch rate can be written as:

$$\frac{1}{\widetilde{A}}\frac{d\widetilde{A}}{d\tilde{t}} = -[\vec{\nabla} \times (\vec{V} \times \vec{n})] \cdot \vec{n} + v_n(\vec{\nabla} \cdot \vec{n}) \tag{2}$$

where $\vec{V}$ is flow velocity and $\vec{n}$ is the unit normal vector of flame surface, v_n is the normal component of the flame front propagating velocity and $\vec{\nabla} \cdot \vec{n}$ is flame curvature. For the steady flames considered in this study, v_n is zero. Therefore, the stretch rate, which only depends on the flow field given by Eqs. (1a) and (1b), becomes

$$\frac{1}{\widetilde{A}}\frac{d\widetilde{A}}{d\tilde{t}} = -\frac{1}{\tilde{r}^N}\frac{d}{d\tilde{r}}(\tilde{r}^N\tilde{u}) = \tilde{k} \tag{3}$$

which indicates that the two flame configurations will have the same stretch rate $\tilde{k}$ if the inlet velocity is specified according to Eqs. (1a,1b). Note that the flame stretch rate $\tilde{k}$ is independent of the inner tube radius $\widetilde{R}_I$. Therefore, by fixing $\tilde{k}$ and varying $\widetilde{R}_I$ for the tubular flame configuration ($N = 1$), flames at the same stretch rate but different curvatures (different flame radii $\widetilde{R}_f$) can be obtained [14,15,17,18,21]. When $\widetilde{R}_I \to \infty$ and $N = 1$, the tubular flame has zero flame curvature and it becomes counterflow flame ($N = 0$); when $\widetilde{R}_I = 0$ and $N = 1$, the flame curvature reaches its maximum value and it is the traditional tubular flame configuration (without the inner tube) employed in previous studies [13–16,20,22]. So the current model is more general and it will be shown that previous results on both counterflow flames and tubular flames can be recovered.

Since we are interested in the dynamics of the near limit flames, the combustible mixture is sufficiently off-stoichiometric so that the flame strength is only determined by the concentration of fuel. By assuming constant density, constant thermal properties, and one-step irreversible chemical reaction, the non-dimensional conservation equations for energy and fuel mass fraction can be written as

$$-k\frac{r^2 - R_I^2}{r}\frac{dT}{dr} = \frac{1}{r^N}\frac{d}{dr}\left(r^N\frac{dT}{dr}\right) + \omega - q_r \tag{4a}$$

$$-k\frac{r^2 - R_I^2}{r}\frac{dY}{dr} = \frac{1}{Le}\frac{1}{r^N}\frac{d}{dr}\left(r^N\frac{dY}{dr}\right) - \omega \tag{4b}$$

The parameters with and without carrot symbol denote the dimensional and non-dimensional variables, respectively. The variables, r, T and Y are, respectively, the axial coordinate, temperature, and fuel mass fraction normalized by $\tilde{\delta}_f^0$, $\widetilde{Y}_\infty\widetilde{Q}/\widetilde{C}_P$, and $\widetilde{Y}_\infty$, where $\tilde{\delta}_f^0 = \tilde{\lambda}/(\tilde{\rho}\widetilde{C}_P\widetilde{S}_L^0)$ is the flame thickness of adiabatic planar flame, $\tilde{\lambda}$ the thermal conductivity, $\tilde{\rho}$ the density, $\widetilde{C}_P$ the specific heat capacity at constant pressure, $\widetilde{Q}$ the reaction heat-release per unit mass of fuel, and $\widetilde{Y}_\infty$ the fuel mass fraction in the fresh mixture.

Additionally, $Le = \tilde{\lambda}/\tilde{\rho}\widetilde{C}_P\widetilde{D}$ is the Lewis number and $\widetilde{D}$ is the mass diffusivity of fuel. The normalized stretch rate is $k = \tilde{k}\tilde{\rho}\widetilde{C}_P(\tilde{\delta}_f^0)^2/[(N+1)\tilde{\lambda}]$. The adiabatic laminar burning velocity $\widetilde{S}_L^0$ for first-order one-step reaction is [25]:

$$\widetilde{S}_L^0 = \left\{ 2 \cdot \frac{\tilde{\lambda}}{\tilde{\rho}\widetilde{C}_P} \cdot \widetilde{B} \cdot \frac{Le}{Z^2} \cdot \exp\left(-\frac{T_a}{T_{ad}}\right) \right\}^{1/2} \tag{5}$$

where $Z = T_a/T_{ad}^2$ is the Zeldovich number, $\widetilde{B}$ the pre-factor of the Arrhenius expression, T_{ad} the normalized adiabatic flame temperature, and T_a the normalized activation temperature.

On the right-hand side of Eq. (4a), q_r is the non-dimensional volumetric radiation heat loss. It is approximated by using the optically thin grey gas model [8]

$$q_r = 4\tilde{\sigma}\widetilde{K}_P(\widetilde{T}^4 - \widetilde{T}_\infty^4)(\tilde{\delta}_f^0)^2\widetilde{C}_P/(\widetilde{Y}_\infty\widetilde{Q}\tilde{\lambda}) \tag{6}$$

where $\tilde{\sigma}$ is the Stefan–Boltzmann constant, $\widetilde{K}_P$ the Planck mean absorption coefficient of the mixture, and $\widetilde{T}_\infty$ the temperature of the incoming fresh mixture.

In the limit of large activation energy, chemical reaction occurs only within a very thin zone of high temperature, whose thickness is much smaller than that of radiation zone [3,8]. Therefore, the reaction rate can be replaced by the Dirac-Delta function [26–28]

$$\omega = \exp\left(\frac{T_a}{2T_{ad}} - \frac{T_a}{2T_f}\right) \cdot \delta(r - R_f) \tag{7}$$

where T_f and R_f are the flame temperature and radius, respectively. By integrating the conservation Eqs. (4a),(4b) around the flame front ($r = R_f$), the jump relations for temperature and fuel mass fraction can be obtained as [26,27]

$$\left.\frac{dT}{dr}\right|_{R_f^-} - \left.\frac{dT}{dr}\right|_{R_f^+} = \frac{1}{Le}\left(\left.\frac{dY}{dr}\right|_{R_f^+} - \left.\frac{dY}{dr}\right|_{R_f^-}\right) = \exp\left(\frac{T_a}{2T_{ad}} - \frac{T_a}{2T_f}\right) \tag{8}$$

The symmetric (for $R_I = 0$) or adiabatic (for $R_I > 0$) condition is used at the inner boundary ($r = R_I$). At the inlet ($r = R_O$), the Hirschfelder boundary condition for the fuel concentration, as suggested by Matthews et al. [20], is used instead of plug flow boundary condition. By defining the flame as the location where fuel concentration goes to zero, the boundary conditions for temperature and fuel mass fraction can be given as

$$r = R_I : \quad dT/dr = 0, \quad dY/dr = 0 \tag{9a}$$
$$r = R_f : \quad T = T_f, \quad Y = 0 \tag{9b}$$
$$r = R_O : \quad T = T_\infty, \quad Le^{-1}dY/dr = k(1 - Y)(r^2 - R_I^2)/r \tag{9c}$$

It should be noted that for counterflow flame ($R_O \to \infty$), the inlet boundary condition (9c) reduces to the plug flow boundary condition ($Y = 1$), which is used in previous theoretical studies of counterflow flames [7].

3. Asymptotic solution

In the limit of large activation energy, it is reasonable to assume that the magnitude of the radiation heat loss term in the energy equation is one-order smaller than those of the convection and diffusion terms. This assumption has been widely used in combustion theory [6,27] and its validity has been confirmed from previous analysis. The radiation term given by Eq. (6) can be written as

$$q_r = h(T^4 - T_\infty^4), \quad h = 4\tilde{\sigma}\widetilde{K}_P\frac{(\tilde{\delta}_f^0)^2\widetilde{Y}_\infty^3\widetilde{Q}^3}{\tilde{\lambda}\widetilde{C}_P^3} << 1 \tag{10}$$

The validity of $h << 1$ will be shown later by Fig. 2. It should be noted that the non-linear radiation heat loss is considered in the present study. It was shown by Ju et al. [10] that the linearized radi-

ation heat loss results in a narrower flammable region and a larger flammability limit compared to nonlinear radiation heat loss model. Therefore, by using the non-linear radiation model, the current model can more accurately demonstrate the dynamics of radiation dominated near-limit flames.

Since the delta-function model for reaction rate is used here, in the limit of large activation energy, the governing equations can be solved analytically in the burned gas ($R_I \leqslant r \leqslant R_f$) and unburned gas ($R_f \leqslant r \leqslant R_O$) regions separately. The fuel mass fraction in the burned gas region is zero according to the fuel lean assumption and that in the unburned gas region is obtained by solving Eq. (4b) together with the boundary conditions in Eqs. (9b), (9c), which gives

$$Y^+(r) = \frac{\int_{R_f}^r \tau^{kLeR_I^2-N}e^{-kLe\tau^2/2}d\tau}{\int_{R_f}^{R_O} \tau^{kLeR_I^2-N}e^{-kLe\tau^2/2}d\tau + [kLe(R_O^2-R_I^2)]^{-1}R_O^{kLeR_I^2-N+1}e^{-kLeR_O^2/2}} \tag{11}$$

Here superscripts '+' and '−' denote the states on the unburned and burned sides of the flame front, respectively. To find the temperature distribution, the energy Eq. (4a) with boundary conditions in Eq. (9) can be solved asymptotically, i.e. $T = T_0 + hT_1 + O(h^2)$, with the accuracy to the first order, $O(h)$. The temperature distribution in the burned gas region ($R_I \leqslant r \leqslant R_f$) is

$$T^-(r) = T_f - h^-(T_f^4 - T_\infty^4)\int_r^{R_f}\left[\int_{R_I}^\tau (s/\tau)^{N-kR_I^2}e^{k(s^2-\tau^2)/2}ds\right]d\tau \tag{12}$$

and that in the unburned gas region ($R_f \leqslant r \leqslant R_O$) is

$$T^+(r) = T_0^+(r) + h^+T_1^+(r) \tag{13a}$$
$$T_0^+(r) = T_\infty + (T_f - T_\infty)G(r)/G(R_f) \tag{13b}$$
$$T_1^+(r) = \frac{G(r)}{G(R_f)}\int_{R_f}^{R_O}\frac{\varphi(s)[T_f - T_0^+(s)]}{dT_0^+(s)/ds}ds - \int_r^{R_O}\frac{\varphi(s)[T_0^+(r) - T_0^+(s)]}{dT_0^+(s)/ds}ds \tag{13c}$$

where $G(r) = \int_r^{R_O}\tau^{kR_I^2-N}e^{-k\tau^2/2}d\tau$ and $\varphi(r) = [T_0^+(r)]^4 - T_\infty^4$.

The gradients of temperature and fuel mass fraction at the flame front can be obtained from their distributions given by Eqs. (11–13). By using the jump relations in Eq. (8), one obtains the following algebraic system of equations for flame radius, R_f, and flame temperature, T_f

$$Le^{-1} \cdot F^+(R_f, Le) = \frac{T_f - T_\infty}{\int_{R_f}^{R_O}(s/R_f)^{kR_I^2-N}e^{k(R_f^2-s^2)/2}ds} + L^+(R_f, T_f) + L^-(R_f, T_f) \tag{14a}$$

$$Le^{-1} \cdot F^+(R_f, Le) = e^{T_a(T_{ad}^{-1} - T_f^{-1})/2} \tag{14b}$$

where

$$F^+(R_f, Le)$$
$$= \frac{R_f^{kLeR_I^2-N}e^{-kLeR_f^2/2}}{\int_{R_f}^{R_O}\tau^{kLeR_I^2-N}e^{-kLe\tau^2/2}d\tau + [kLe(R_O^2-R_I^2)]^{-1}R_O^{kLeR_I^2-N+1}e^{-kLeR_O^2/2}} \tag{15a}$$

$$L^+(R_f, T_f) = h^+\frac{\int_{R_f}^{R_O}\varphi(\tau)\left[\int_\tau^{R_O}(s/\tau)^{kR_I^2-N}e^{k(\tau^2-s^2)/2}ds\right]d\tau}{\int_{R_f}^{R_O}(s/R_f)^{kR_I^2-N}e^{k(R_f^2-s^2)/2}ds} \tag{15b}$$

$$L^-(R_f, T_f) = h^-(T_f^4 - T_\infty^4) \cdot \int_{R_I}^{R_f}(s/R_f)^{N-kR_I^2}e^{k(s^2-R_f^2)/2}ds \tag{15c}$$

Eqs. (14) and (15) yield a general solution for both tubular flames ($N = 1$) and counterflow flames ($N = 0$). The solution of flame radius, R_f, and flame temperature, T_f, as a function of stretch rate, k, can be obtained by solving the above equations numerically for different h, R_I, R_O, N and Le. The flame speed, which is equal to

flow speed at the flame front, can be calculated from flame radius and the potential flow field given by Eq. (1). According to Eq. (14b), the term on the left-hand side of Eq. (14a) denotes the total chemical heat release. The first term on the right-hand side of Eq. (14a) represents the heat flux induced by thermal conduction to the unburned side, while the second and third term represent heat flux induced by radiation heat losses in the unburned and burned regions, respectively. The adiabatic flame temperature of stretched flames can be obtained by setting the radiation heat loss ($L^{\pm}$ or $h^{\pm}$) to be zero.

Eqs. (14) and (15) reduce to the previous results of adiabatic tubular flames [20] in the limit of $N = 1$, $R_I = 0$, and $L^{\pm} = 0$; and those of counterflow flames [3,10] in the limit of $N = 0$, $R_I = 0$, and $R_O \rightarrow \infty$. Furthermore, by specifying $R_I > R_O$ (now the outer tube is of radius R_I while the inner one of radius R_O), solutions to tubular flames of negative curvature (unlike the tubular flame of positive curvature shown in Fig. 1(a), a tubular flame of negative curvature is established when combustible mixture is injected toward the outer tube through the porous inner tube) can be obtained from the current results.

4. Results and discussion

The current results, Eqs. (14) and (15), provide a general theoretical description of flame speed, flame temperature and extinction limits. By specifying different flame curvatures (by changing R_I or N), flame stretches (by changing k), and radiation heat loss intensities (by changing fuel concentration or the concentrations of radiative gases, $h^{\pm}$), the effects of flame curvature, radiation, and stretch rates can be systematically investigated. Furthermore, the preferential diffusion effect can be demonstrated by comparing results at different Lewis numbers (by changing Le).

In the following calculations, the integrations in Eqs. (14) and (15) are evaluated by using QUADPACK [29] and the thermal and chemical parameters are chosen to mimic methane/air mixture. They are $\widetilde{Q} = 4.75 \cdot 10^7$ J/kg, $\widetilde{C}_P = 1400$ J/kg/K, $\widetilde{B} = 2.5 \cdot 10^{10}$ m³/mol/s, $\tilde{\rho} = 1.0$ kg/m³, $\widetilde{T}_{\infty} = 300$ K, $\widetilde{T}_a = 25000$ K, $\widetilde{K}_P = 2.0$ m^{-1}, and $\tilde{\lambda}/(\tilde{\rho}\widetilde{C}_P) = 5 \cdot 10^{-5}$ m²/s. The Lewis number of methane/air flames is close to unity. Therefore unit Lewis number is utilized in the followings except in the last subsection, in which the effects of Lewis number is investigated and different Lewis numbers could be obtained by adding Helium into the methane/air mixture [30].

The variation of normalized radiation coefficient h (Eq. (10)) with the fuel mass fraction in fresh mixture is shown in Fig. 2.
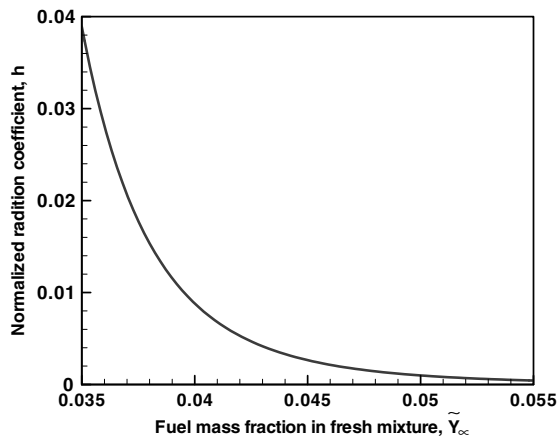
Since h is proportional to the inverse of the square of flame speed, it is seen that h deceases exponentially with the increase of $\widetilde{Y}_{\infty}$, which means that radiation is the dominant factor for near limit flames and becomes much less important for mixtures near stoichiometric conditions. Moreover, Fig. 2 shows $h < 0.04$ for all the initial fuel mass fractions $\widetilde{Y}_{\infty}$ studied here. Therefore the assumption of $h \ll 1$ used in the asymptotic analysis is reasonable. In the following, the effects of flame curvature, radiation, stretch, and Lewis number on flame extinction will be discussed. Note that the outer tube radius is set to be infinity ($R_O = \infty$), so the heat conduction to the outer tube, which was studied by Kobayashi et al. [15] and Matthews et al. [20], is not considered here. Besides, in the present study and all previous studies, the surface radiation is not considered in the tubular geometry. The existence of the inner and outer tubes could interact with the gas-phase radiation losses. This is a subject for future study.

4.1. Flame extinction and bifurcations of tubular flames

It is well known that radiation heat loss depends strongly on the volume of the hot emitting gas. Therefore, the appearance of flame curvature in tubular flame yields a smaller volume of the burned gas per unit area of the flame front than that of the planar counterflow flame. As a result, an increase of flame curvature reduces the radiation heat loss and thus improves the combustion. On the other hand, an increase of flame curvature increases the heat conduction loss from the burned gas side to the unburned gas side (caused by the so-called defocusing effect) and the flame speed is decreased. So flame curvature also weakens the flame strength. The above two competing effects of flame curvature, together with that of radiation will be shown to greatly affect the flame extinction.

To quantitatively evaluate the effect of radiation heat loss, the fraction of radiation heat loss is introduced [8,12]:

$$Fr = \int_{R_I}^{R_O} q_r (2\pi r)^N \mathrm{d}r \Big/ \int_{R_I}^{R_O} \omega (2\pi r)^N \mathrm{d}r$$
$$= \int_{R_I}^{R_O} q_r (2\pi r)^N \mathrm{d}r \Big/ [(2\pi R_f)^N e^{T_a(T_{ad}^{-1} - T_f^{-1})/2}] \quad (16)$$

where the numerator denotes the total radiation heat loss in both the unburned and burned zones and the denominator denotes the total chemical heat release rate.

Fig. 3 shows the dependences of flame radius, flame temperature and fraction of radiation heat loss of tubular flames ($R_I = 0, R_O = \infty, N = 1$) on stretch rate at $Le = 1.0$ and $\widetilde{Y}_{\infty} = 0.0376$. It is seen that the non-adiabatic tubular flames exhibit an isola response, with dual extinction limits at higher and lower values of stretch rate (b and d). According to previous stability analysis mentioned in [20], the branch of large flame radius (thus large flame speed) is stable (solid lines in Fig. 3) while the branch of small flame radius (thus small flame speed) is unstable (dashed lines in Fig. 3).

It is seen that the mixture can burn in a range of stretch rate between 1.3 s^{-1} and 6.7 s^{-1}. For stretch rates larger than 3.5 s^{-1} (point a), an increase of the stretch rate causes the decrease of flow residence time and flame radius. Therefore, the fraction of radiation heat loss decreases and flame temperature increases. Flame extinction occurs at point b. For counterflow flames, this extinction is usually called stretch-induced extinction limit [3–10]. However, for tubular flames the flame curvature (inverse of flame radius) reaches its maximum value at the extinction point b and thus the curvature effect might also help to accelerate flame extinction. The validity of this conclusion will be proved in the next section.

On the other hand, with the decrease of stretch rate (from point a to c to d), the flow residence time increases, which enhances the

Fig. 2. The dependence of radiation coefficient on the fuel mass fraction in fresh mixture.
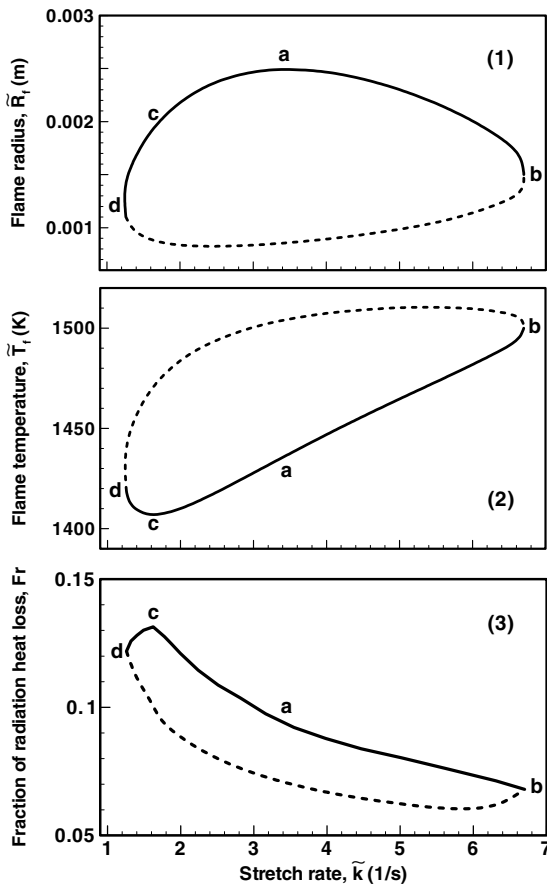
Fig. 3. Dependences of flame radius (1), flame temperature (2), and fraction of radiation heat loss (3) of tubular flames ($R_I = 0$, $R_O = \infty$, $N = 1$) on stretch rate for mixture of $Le = 1.0$ and $\widetilde{Y}_\infty = 0.0376$.
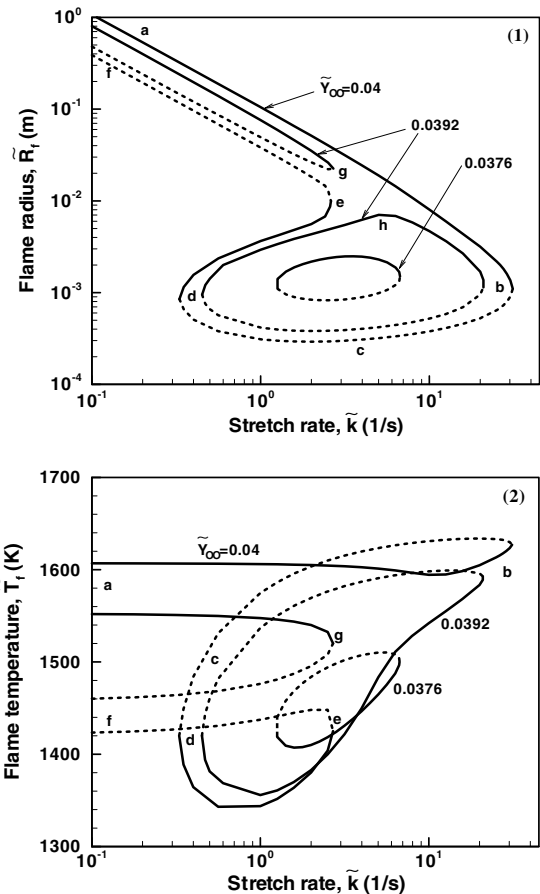

Fig. 4. Flame radius (1) and flame temperature (2) of tubular flames ($R_I = 0$, $R_O = \infty$, $N = 1$) as a function of stretch rate for mixtures of different fuel mass fractions and $Le = 1.0$.

radiation heat loss; while the flame curvature also increases, which reduces radiation by decreasing the volume of radiation emitting gas. The two processes compete with each other and result a non-monotonic change of radiation fraction and flame temperature, as shown in Fig. 3. From point *a* to *c*, the effect of residence time dominates and thus radiation fraction increases and flame temperature decreases; from point *c* to *d*, the effect of curvature dominates and thus radiation fraction decreases and flame temperature increases. The flame is eventually quenched at point *d*. Therefore, unlike the counterflow flame whose low stretch rate extinction limit is only caused by an increase of radiation, that of tubular flame is caused by the combined effects of flame curvature and radiation. Therefore, both the stretch and radiation extinction limits of tubular flames are strongly affected by flame curvature.

Results of tubular flames at other fuel concentrations ($\widetilde{Y}_\infty = 0.0392, 0.04$) are shown in Fig. 4 in order to demonstrate the effect of different radiation intensities ($h = 0.017$, $0.011, 0.009$ for $\widetilde{Y}_\infty = 0.0376, 0.0392, 0.04$, respectively). Different flame regimes are predicted. For $\widetilde{Y}_\infty = 0.0376$, the flammable region is an isola with flame position near the stagnation line ($r = 0$). This is usually called Near Stagnation Flame (NSF). However, with the increase of fuel concentration and thus decrease of radiation heat loss intensity, Fig. 4 shows that there are two distinct flame branches for $\widetilde{Y}_\infty = 0.0392$: one branch is a NSF similar to that of $\widetilde{Y}_\infty = 0.0376$, the other one is far from the stagnation line and thus is called a FSF. For both branches, the sold lines stand for stable solutions while the dashed lines are unstable solutions. With the decrease of radiation heat loss intensity *h* (or increase of $\widetilde{Y}_\infty$), the flame can survive radiation from emitting volume much larger

than that of NSF, which is the reason why the FSF appears. With further decrease of radiation heat loss intensity, the strength of FSF increases and its extinction limit moves to the higher stretch rate side. At the same time, the NSF is also strengthened and it can survive despite the larger radiation emitting volume (thus large $\widetilde{R}_f$). Therefore flame branch bifurcations appear with the increase of fuel concentration (decrease of radiation heat loss intensity). Fig. 4 shows that, for $\widetilde{Y}_\infty = 0.04$, the FSF branch *ag* and NSF branch *hb* merge with each other to form branch *ab*, and so do the FSF branch *fg* and NSF branch *hd* to form branch *fed*. It is seen that for $\widetilde{Y}_\infty = 0.04$ there are two stable solutions for stretch rate between 0.33 s^{-1} and 2.72 s^{-1}, of which the one of higher temperature (on *ab* branch) is call normal flame, while the one of lower temperature (on *de* branch) is called the weak flame [9,22].

Similar flame bifurcations shown in Fig. 4 have also been found in the detailed numerical simulation of tubular and counterflow methane-air flames [8,22] and theoretical analysis of counterflow flames [6], which confirms the validity of the current general theoretical description of the combined effects of flame curvature, radiation, and stretch given by Eqs. (14) and (15). The different flame regions of counterflow flames predicted by the current theoretical correlation is the same as those shown in Buckmaster's analysis [6] and thus are not repeated here.

4.2. Curvature and radiation effects on extinction limits

To further study the combined effect of flame curvature and radiation, the tubular flames of different inner tube radii $\widetilde{R}_I$ are studied for mixture of $Le = 1.0$ and $\widetilde{Y}_\infty = 0.0376$. The dependence
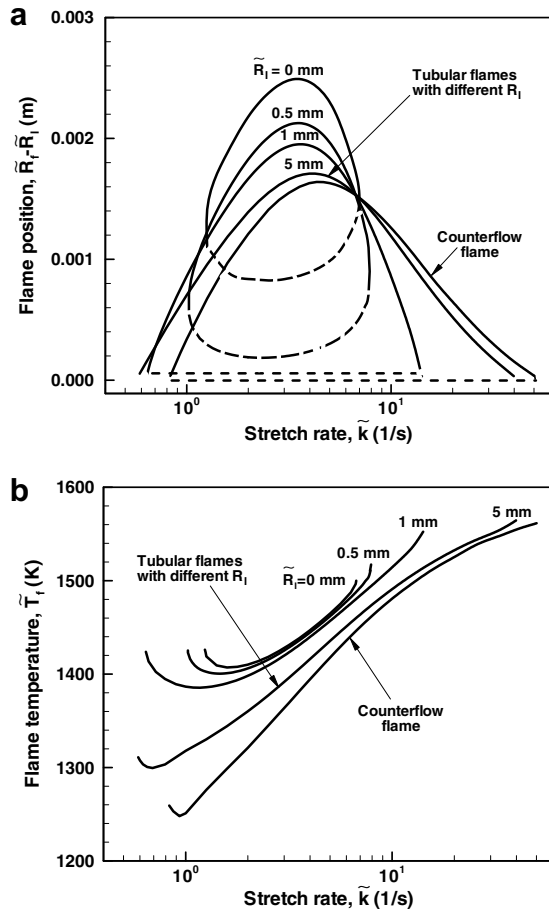
Fig. 5. Flame radius (a) and flame temperature (b) as a function of stretch rate for tubular flames ($N = 1$, different R_I) and counterflow flames ($N = 0$) at $Le = 1.0$, $\widetilde{Y}_\infty = 0.0376$, and $R_O = \infty$.

of flame position (stable branches in solid lines and unstable branches in dashed lines) and flame temperature (only stable branches) on stretch rate are shown in Fig. 5. It is seen that by continuously increasing the inner tube radius, the isola response for counterflow flames is recovered. Note that the flame position $\widetilde{R}_f - \widetilde{R}_I$ and the flame temperature are strongly affected by the inner tube size. Flame position $\widetilde{R}_f - \widetilde{R}_I$ and flame temperature both increase with the increase of flame curvature (decrease of $\widetilde{R}_I$) since flame curvature reduces the radiation heat loss.
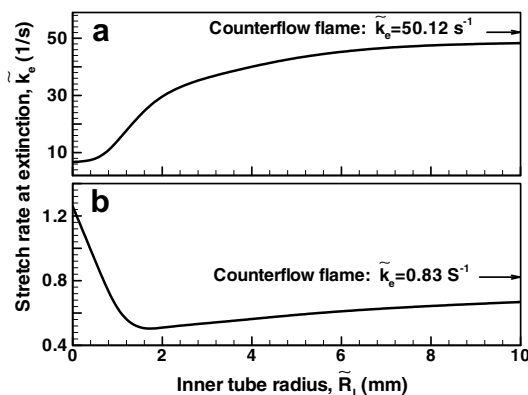

Fig. 6. Stretch rate at extinction limits as a function of inner tube size for tubular flames and counterflow flame at $Le = 1.0$, $\widetilde{Y}_\infty = 0.0376$, and $R_O = \infty$.

Furthermore, the flame position, flame temperature, and stretch rate at both extinction limits are significantly changed by choosing different inner tube radii. As shown in Fig. 6, the stretch rate at the upper extinction limit (stretch extinction limit) decreases *monotonically* with the increase of flame curvature (decrease of the inner tube radius). However, it is interesting to note that the dependence of the lower extinction limit (radiation extinction limit) on flame curvature is *not monotonic*. Similar non-monotonic dependences for flame position and flame temperature on flame curvature at the radiation extinction limits can also be seen in Fig. 5. This result shows that flame curvature and radiation coupling has distinct effects on the stretch extinction limit and the radiation extinction limit.

For extinction at high stretch rate, when the inner tube radius is large, flame is very close to the stagnation surface ($\widetilde{R}_f - \widetilde{R}_I \approx 0$ for $\widetilde{R}_I = 1, 5$ mm in Fig. 5) and the radiation fraction reaches its minimum value (according to Fig. 3(3)). So the radiation effect at upper extinction limit could be negligible. This is further confirmed by the nearly constant flame temperature at the stretch extinction limit for different $\widetilde{R}_I$ shown in Fig. 5. Therefore, the change of extinction stretch rate is purely caused by flame curvature. When the inner tube radius is smaller than *1* mm, the $\widetilde{R}_f - \widetilde{R}_I$ at extinction increases significantly with decrease of $\widetilde{R}_I$, and then flame temperature decreases because of the increase of radiation heat loss. Therefore, the change of extinction stretch rate is caused by combined effects of flame curvature and radiation.

For extinction at low stretch rate, flame extinction is also caused by the combined effects of flame curvature and radiation. As mentioned before, an increase of flame curvature has two effects: (1), the reduction of the radiation heat loss and consequent improvement in combustion; and (2), the decrease of flame speed and consequent reduction in the flame strength. The two processes compete with each other in the determination of the low stretch rate extinction limits. For large inner tube radius ($\widetilde{R}_I > 1.6$ mm), the first effect dominates, thus the stretch rate at extinction decreases with the increase of flame curvature (decrease of inner tube size); while for small inner tube radius ($\widetilde{R}_I < 1.6$ mm), the second effect dominates, thus the stretch rate at extinction increases with the increase of flame curvature (decrease of inner tube size).

Therefore, flame curvature has significant effects on extinction of premixed tubular flames since the extinction limits can be greatly changed by choosing different inner tubes to change flame curvature. Note that all the cases studied above are for mixtures of $Le = 1.0$, so the stretch effect caused by preferential diffusion is not covered. The Lewis number effect will be demonstrated in the next section.

4.3. Effects of preferential diffusion (Lewis number effect)

The impact of radiation and flame curvature coupling on near limit flames will be enriched by the appearance of preferential diffusion. The effects of Lewis number on the tubular flames are shown in Fig. 7. It can be seen that the flammable region is greatly expanded by decrease of Lewis number. With decrease in the Lewis number, the stretch rate at upper limit increases while that at lower limit decreases. Furthermore, the flame radius decreases and flame temperature increases with the decrease of Lewis number at both extinction limits. This effect can be easily understood from Eq. (14). Eq. (14) shows that the lower the Lewis number, the higher the adiabatic flame temperature and thus flame can survive much larger radiation heat loss and flame curvature. Note that the flame temperature increase at upper extinction limit is much larger than that at lower extinction limit. This is because the Lewis number effect is proportional to the magnitude of stretch rate. Similar results for counterflow flames are also obtained from the current theory and are consistent with those of the previous study [10].
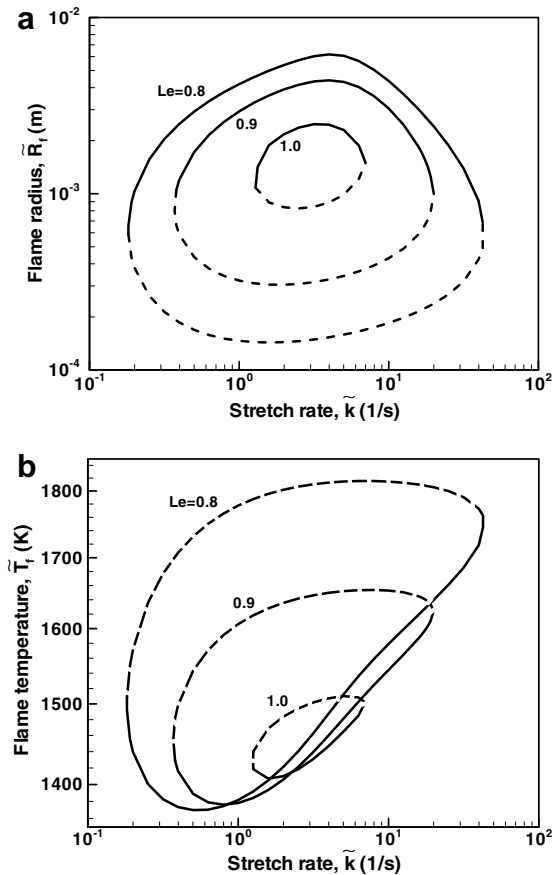
Fig. 7. Flame radius (a) and flame temperature (b) of tubular flames ($R_I = 0$, $R_O = \infty$, $N = 1$) as a function of stretch rate for mixtures of $\tilde{Y}_\infty = 0.0376$ and different Lewis numbers.

To demonstrate further the effect of Lewis number, radiation, and curvature on the extinction of tubular flames, the stretch rates at two different extinction limits for different inner tube radii and Lewis numbers are shown in Fig. 8. For fixed inner tube radius, the Lewis number effect is the same: the stretch rate at upper limit increases while that at lower limit decreases with the decrease of Lewis number. Therefore, the preferential diffusion of mass over heat ($Le < 1$) extends the flammable region for all the tubular flames with different curvatures. For fixed Lewis number, the stretch rate
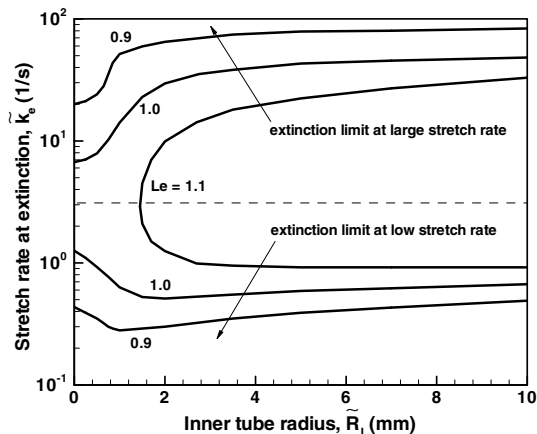

Fig. 8. Stretch rate at extinction limits as a function of inner tube size for tubular flames at $\tilde{Y}_\infty = 0.0376$, and $R_O = \infty$.

at the upper stretch extinction limit decreases monotonically. However, depending on the Lewis number, the radiation extinction limit can be either monotonically or non-monotonically dependent on the flame curvature. At large Lewis numbers (e.g. $Le = 1.1$), the stretch effect is dominant. Therefore an increase of flame curvature leads to a monotonical increase of the extinction limit. There is a critical curvature above which no premixed tubular flames could be obtained (for $Le = 1.1$, no solution for $R_I < 1.5$ mm). However, at lower Lewis numbers (e.g. $Le = 0.9$ and 1.0), the effect of radiation and flame curvature coupling becomes dominant. The radiation extinction limit depends non-monotonically on the flame curvature. In addition, flame curvature does not lead to flame extinction. As shown in Fig. 8, at a large flame radius, the decrease of flame radius causes a decrease (or broadening) of extinction limit. As the flame curvature increases, the radiation extinction limit reaches a minimum value. A further increase of flame curvature causes an increase of the extinction limit. Therefore, there is a critical Lewis number which separates the monotonic and non-monotonic curvature dependence regimes. This critical Lewis number will be larger than unity and increases with the increase of radiation intensity.

5. Conclusions

The flame dynamics of near limit premixed tubular flames are studied by using the large activation energy asymptotic method. A general correlation for flame speed, flame temperature and extinction limits is obtained and it is used to study the combined effects of flame curvature, radiation, and stretch on flame extinction. The following conclusions are made:

1. The coupling between radiation and flame curvature leads to multiple flame bifurcations and extinction limits at different radiation intensities (different fuel mass concentrations). For mixtures with high radiation intensity, the flammable region is an isola and only the NSF is observed. With the decrease of radiation heat loss intensity, two distinct flame branches, NSF and FSF, are first predicted and then they will merge with each other.
2. It is shown that both the stretch and radiation extinction limits are strongly affected by flame curvature. The stretch extinction limit is found to monotonically decrease with the increase of flame curvature. However, depending on the Lewis number, the radiation extinction limit can be either monotonically or non-monotonically dependent on the flame curvature. For Lewis numbers larger than a critical Lewis number, the increase of flame curvature results in a monotonic increase of the extinction limit and there is a critical curvature at which flame extinguishes. For Lewis numbers smaller than the critical value, the increase of flame curvature leads to a non-monotonic dependence of the radiation extinction limit and flame curvature does not lead to flame extinction.

References

[1] D.B. Spalding, A theory of inflammability limits and flame-quenching, Proc. R. Soc. London, Ser. A 240 (1957) 82–100.

[2] J. Buckmaster, The quenching of deflagration waves, Combust. Flame 26 (1976) 151–162.

[3] S.H. Sohrab, C.K. Law, Extinction of premixed flames by stretch and radiative loss, Int. J. Heat Mass Trans. 27 (1984) 291–300.

[4] K. Maruta, M. Yoshida, Y. Ju, T. Niioka, Experimental study on methane–air premixed flame extinction at small stretch rates in microgravity, Proc. Combust. Inst. 26 (1996) 1283–1289.

[5] C.J. Sung, C.K. Law, Extinction mechanisms of near-limit premixed flames and extended limits of flammability, Proc. Combust. Inst. 26 (1996) 865–873.

[6] J. Buckmaster, The effects of radiation of stretched flames, Combust. Theory Modell. 1 (1997) 1–11.

[7] H. Guo, Y. Ju, K. Maruta, T. Niioka, F. Liu, Radiation extinction limit of counterflow premixed lean methane–air flames, Combust. Flame 109 (1997) 639–646.

[8] Y. Ju, H. Guo, K. Maruta, F. Liu, On the extinction limit and flammability limit of nonadiabatic stretched methane-air premixed flame, J. Fluid Mech. 342 (1997) 315–334.

[9] Y. Ju, H. Guo, F. Liu, K. Maruta, Effects of the Lewis number and radiative heat loss on the bifurcation and extinction of CH_4/O_2-N_2-He flames, J. Fluid Mech. 379 (1999) 165–190.

[10] Y. Ju, G. Masuya, F. Liu, Y. Hattori, D. Riechelmann, Asymptotic analysis of radiation extinction of stretched premixed fames, Int. J. Heat Mass Transfer 43 (2000) 231–239.

[11] F. Liu, G.J. Smallwood, Ö.L. Gülder, Y. Ju, Asymptotic analysis of radiative extinction in counterflow diffusion flames of nonunity Lewis numbers, Combust. Flame 121 (2000) 275–287.

[12] Z. Chen, Y. Ju, Theoretical analysis of the evolution from ignition kernel to flame ball and planar flame, Combust. Theory Modell. 11 (2007) 427–453.

[13] T. Takeno, S. Ishizuka, A tubular flame theory, Combust. Flame 64 (1986) 83–98.

[14] T. Takeno, M. Nishioka, S. Ishizuka, A theory study of extinction of a tubular flame, Combust. Flame 66 (1986) 271–283.

[15] H. Kobayashi, M. Kitano, Extinction characteristics of stretched cylindrical premixed flame, Combust. Flame 76 (1989) 285–295.

[16] H. Kobayashi, M. Kitano, Effects of equivalence ratio on the extinction stretch rate of cylindrical premixed flames, Combust. Sci. Technol. 89 (1993) 253–263.

[17] D.M. Mosbacher, J.A. Wehrmeyer, R.W. Pitz, C.J. Sung, J.L. Byrd, Experimental and numerical investigation of premixed tubular flames, Proc. Combust. Inst. 29 (2002) 1479–1486.

[18] P. Wang, S. Hu, J.A. Wehrmeyer, R.W. Pitz, Stretch and curvature effects on flames, 42nd AIAA Aerospace Sciences Meeting, 2004, No. AIAA-2004-0148.

[19] P. Wang, J.A. Wehrmeyer, R.W. Pitz, Stretch rate of tubular premixed flames, Combust. Flame 145 (2006) 401–414.

[20] M.T. Matthews, B.Z. Dlugogorski, E.M. Kennedy, The asymptotic structure of premixed tubular flames, Combust. Flame 144 (2006) 838–849.

[21] T. Yokomori, Z. Chen, Y. Ju, Studies on the flame curvature effect on burning velocity, 44th AIAA Aerospace Sciences Meeting and Exhibit, 2006, No. AIAA-2006-0161.

[22] Y. Ju, H. Matsumi, K. Takita, G. Masuya, Combined effects of radiation, flame curvature, and stretch on the extinction and bifurcations of cylindrical CH_4/air premixed flame, Combust. Flame 116 (1999) 580–592.

[23] F.A. Williams, A review of some theoretical considerations of turbulent flame structure, Agard Conference Proceedings, No.164, 1975, pp. 1–25.

[24] M. Matalon, On flame stretch, Combust. Sci. Technol. 31 (1983) 169–181.

[25] I. Glassman, Combustion, third ed., Academic Press, 1996.

[26] G.I. Sivashinsky, Diffusional-thermal theory of cellular flames, Combust. Sci. Technol. 15 (1977) 137–146.

[27] G. Joulin, P. Clavin, Linear stability analysis of nonadiabatic flames: diffusional-thermal model, Combust. Flame 35 (1979) 139–153.

[28] C.K. Law, Combustion Physics, Cambridge University Press, 2006.

[29] R. Piessens, E. Doncker-Kapenger, C. Ueberhuber, D. Kahaner, QUADPACK, a Subroutine Package for Automatic Integration, Springer Verlag, 1983.

[30] Z. Chen, X. Qin, B. Xu, Y. Ju, F. Liu, Studies of radiation absorption on flame speed and flammability limit of CO_2 diluted methane flames at elevated pressures, Proc. Combust. Inst. 31 (2007) 2693–2700.